J Mater Sci: Mater Electron (2016) 27:9734–9739
DOI 10.1007/s10854-016-5036-x

Structural and magnetic properties of CuCo films electrodeposited in the presence of trisodium citrate

F. R. de Paula[1] · A. L. Oestereich[2] · L. A. Zago[3] · E. R. Spada[3]

Received: 18 February 2016 / Accepted: 21 May 2016 / Published online: 26 May 2016

Abstract The structure and magnetic properties of CuCo alloys electrodeposited in aqueous solution on n-type Si(100) substrates were investigated as a function of the trisodium citrate concentration in the electrolyte. The compositional analysis show that percentage of Co has a non-monotonic dependence on the increase in concentration of sodium citrate, with a maximum at 300 mM followed by a significant decrease The magnetic measurements in similar samples in terms of composition and thickness show that the coercive field value it differs greatly, from 87 to 20 Oe without and with added citrate, respectivelly, owing to the improved morphological quality and change in crystalline structure induced by the citrate. For electrodeposited films without citrate in the electrolyte, the X-ray diffraction pattern shows two peaks at $2\theta = 43.298$ and 44.217 typical of fcc (111) planes for copper and cobalt, respectively, while in the presence of citrate only one peak characteristic of fcc of the CuCo alloy was observed.

✉ E. R. Spada
edspada@gmail.com

[1] Departamento de Física e Química, Universidade Estadual Paulista Júlio de Mesquita Filho, Caixa Postal 31, Ilha Solteira, SP 15385-000, Brazil

[2] Departamento de Física, Universidade Federal de Santa Catarina, Caixa Postal 476, Florianópolis, SC 88040-900, Brazil

[3] Grupo de Polímeros Bernard Gross, Instituto de Física de São Carlos, Universidade de São Paulo, Caixa Postal 369, São Carlos, SP 13560-970, Brazil

1 Introduction

CuCo alloys are promising for data storage systems and sensing [1, 2], owing to their giant magneto resistance [3–6] through which a large change in electrical resistance is induced by an external magnetic field. These alloys may be produced via electrodeposition, which is advantageous for being inexpensive compared to other complex, sophisticated methods such as magnetron sputtering [7]. Depending on the preparation conditions, *i.e.* electrolyte composition, pH, temperature, current density and additives, films can be obtained with varied morphological and structural properties [8, 9]. The atomic arrangement of alloys can be modified by incorporation of elements with a different crystalline symmetry. Since Cu tends to crystallize in an fcc structure, its incorporation into the Co structure is expected to favor formation of CuCo alloys with a cubic structure. The control of the crystal structure is essential for tuning the magnetic properties of CuCo alloys [10–12]. Indeed, a slight difference in preparation may cause large changes in the electrodeposited film properties [11–15].

Understanding the deposition mechanism is crucial to control the properties of alloy deposits, especially because additives, such as the complexing agent trisodium citrate, may inhibit crystal growth and catalysis, leading to bright deposits and decreasing the over potential of metal electrodeposition. Trisodium citrate in the electrolyte leads to a series of soluble complex species [16–18], with $CuCit^-$ and $CoCit^-$, in addition to the non-complexed Co^{2+} and Cu^{2+}, being the most prominent. Therefore, CuCo alloys can be obtained by electrodeposition of either the complexed and non-complexed species simultaneously as follows:

$$Cu^{2+} + 2e^- \leftrightarrow Cu$$
$$Co^{+2} + 2e^- \leftrightarrow Co$$
$$Cu\ cit^- + 2e^- \leftrightarrow Cu + cit^{3-}$$
$$Co\ cit^- + 2e^- \leftrightarrow Co + cit^{3-}$$

In this study, we analyze the effects of trisodium citrate concentration on the dynamics of electrodeposition and on the magnetic and structural properties of CuCo alloys. We show that an optimum citrate concentration exists for which the electrodeposited films display superior magnetic properties compared to the films without citrate.

2 Experimental section

Film electrodeposition was carried out at room temperature in a dark chamber, using a three electrode cell with a galvanostat/potentiostat AUTOLAB PGSTAT302 N. An n-type silicon (100) with resistivity of 5–10 Ω was used as working electrode with electroactive area of 0.496 cm^2. A platinum foil was used as counter electrode and the reference was a saturated calomel electrode (SCE). For film electrodeposition, an aqueous solution of 300 mM $CoSO_4.7H_2O$ and 3 mM $CuSO_4.5H_2O$ was used, at a deposition potential of −0.95 and −1.0 V versus SCE (potential measured vs. saturated calomel electrode). Trisodium citrate ($Na_3C_6H_5O_7$) was used as complexing agent, with varying concentration from 0 to 600 mM. The estimated thickness (by Coulometry) is 140 nm for all samples. Cyclic voltammetry was performed with a scan rate of 10 mVs^{-1}, sweeping initially the negative potential. The crystalline structure was analyzed by X-ray diffraction (XRD) on a diffractometer model X'Pert Pro Multi-Purpose, PanAnalytical, where the X-ray source was Cu $K_{\alpha 1}$ radiation ($\lambda = 1.540562$ Å), powered at 40 kV and 30 mA. Measurements were performed in 2θ configuration with the incident beam fixed at 12°, and 2θ between 20° and 100°. In order to increase the signal–noise ratio, each measure presented is the sum of 30 scans. The film composition was obtained by Energy Dispersive X-ray Microanalysis (EDX) and surface morphology images were obtained in the secondary (SE) acquisition mode with a Phillips XL30 scanning electron microscope (SEM). Magnetic characterization was carried out at room temperature in a vibrating sample magnetometer (VSM model EV9 Microsense) in the field range of ±10 kOe.

3 Results and discussion

The effect of trisodium citrate complexing agent on the film properties was studied for the range between 0 and 600 mM in the electrolyte, with the concentrations of Cu and Co ions fixed at 3 and 300 mM, respectively. The cyclic voltammograms in Fig. 1a display an increase in current in two regions in the cathodic scan. The increases in regions I and II are ascribed to deposition of Cu and onset of Co deposition, respectively. For both regions, the potential shifts to more negative values with increasing concentrations of trisodium citrate. The reduction of copper (cobalt) begins at −0.35 (−0.75) V versus SCE in a solution containing only sulphates (squares). Adding trisodium citrate (circles and triangles) shifts the reduction potential of the metal species to more negative values. This is explained by complex formation between Cu^{2+} (Co^{2+}) ions and trisodium citrate, such as $CuCit^-$ ($CoCit^-$), which cannot be reduced as easily as the free metal ions, requiring more negative potentials [19–21]. The addition of trisodium citrate also affected the potentiostatic transient deposition for the CuCo alloy at V = −0.95 V versus SCE, as indicated in Fig. 1b. The deposited charge in the three situations was 200 mC, with a reduction in growth kinetics upon increasing the trisodium citrate concentration, as shown in the inset. Therefore, we expect to obtain higher quality, homogeneous deposits. The same behavior was observed for V = −1.00 V versus SCE, but the saturation currents were −11.0 and −2.2 mA for the electrolytes with no citrate and with 300 mM, respectively. The expectation of more homogeneous films in the presence of the citrate complexing agent was fulfilled, according to the SEM images in Fig. 1c through 1e. Without citrate, a submicrometer granularity is observed in the highly magnified SEM image in Fig. 1c. In contrast, a finer granularity is seen with the complexing agent; even with only 10 mM there is a smoothing effect (Fig. 1d). Visually, the samples in Fig. 1d, e have a highly reflective surface, while the one manufactured without citrate (Fig. 1c) exhibits an opaque surface.

Film composition is known to be affected by the deposition potential [15, 19, 22], and the ratio of the two metals in the film should be different from that in the electrolyte, since it depends on other factors, such as the overpotential that varied with the concentration of the complexing agent (Fig. 1a). Figure 2a shows the variation of Co content (wt%) in the electrodeposited samples due to the citrate concentration added to the electrolyte for the deposition potentials of −0.95 V versus SCE (circles) and −1.00 V versus SCE (squares). In particular, the samples produced at −1.00 V versus SCE with no citrate had 77.5 wt% of cobalt, while the addition of only 2 mM citrate in the electrolyte decreased the cobalt percentage to 25 wt%. Furthermore, the percentage of Co has a non-monotonic dependence on the increase in concentration of sodium citrate, with a maximum at 300 mM followed by a significant decrease at higher concentrations. In addition to changing film composition, varying the citrate

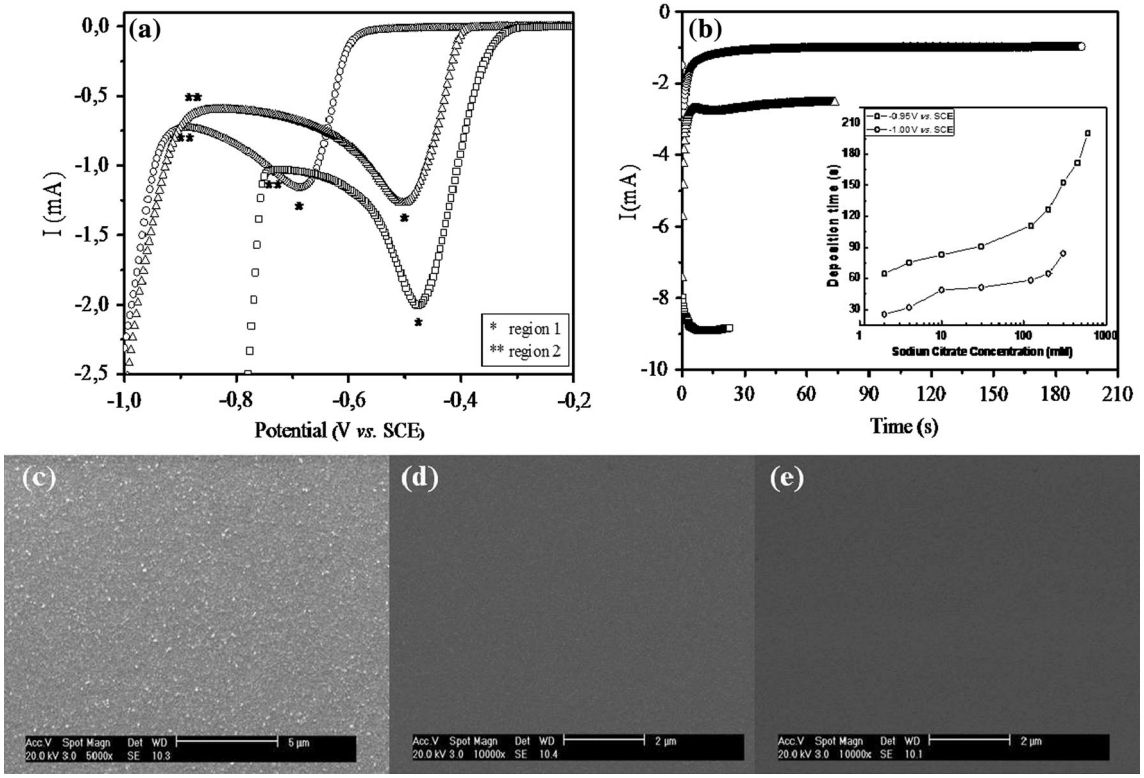

Fig. 1 *Above*; **a** Cyclic voltammetry of CuCo electrolyte in the absence (*square*) and with addition of 10 mM trisodium citrate (*triangle*) and 300 mM (*circle*). **b** Current transients recorded during electroplating. *Inset*: dependence of the deposition time to achieve charge of the 200 mC with the amount of sodium citrate present in the electrolyte. *Below*; SEM images obtained at acquisition modes of secondary electrons (SE) for **c** without, **d**, **e** with the addition of 10 and 300 mM trisodium citrate, respectively

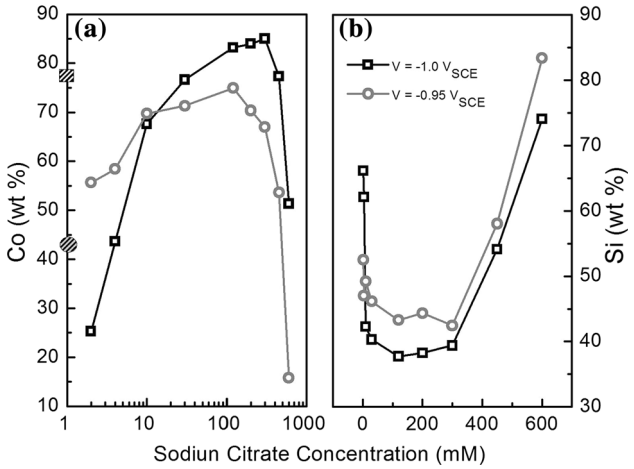

Fig. 2 **a** Variation of Co in the electrodeposited thin films due to the citrate concentration contained in the electrolyte for potential deposition values of −0.95 V versus SCE (*circles*) and −1.00 V versus SCE (*squares*). The circle (*square*) on the axis Co (wt%) represents the amount of cobalt obtained for the sample produced from free citrate electrolyte to −0.95 V versus SCE and −1.00 V versus SCE, respectively. **b** Detected percentage of Si with the increase of the citrate contents

concentration also affected film thickness, which could be inferred from the EDX analysis by determining the Si fraction because the measurements were carried out sequentially, with the same energy (12 keV) and spot size for the electron beam.

In the analysis of the magnetic properties, we chose to normalize the hysteresis loops because we did not determine the mass of magnetic material in the samples, on which properties such as saturation magnetization depend. And we know that varying the concentration of citrate affects the amount of Co in the film (Fig. 2a) and the film growth process (Fig. 2b). The skewed hysteresis loop for the film without citrate in Fig. 3a indicates that the easy axis of magnetization is out of plane and that the in-plane magnetization occurs by spin rotation. The addition of citrate leads to a square hysteresis and lower coercive field, thus pointing to the progressive formation of a film with an in-plane magnetization. A summary of the results is shown in Table 1. We should also mention the specific behavior of two samples with percentages of Co 77 % (no citrate) and 77 % (30 mM citrate), which also have similar thicknesses

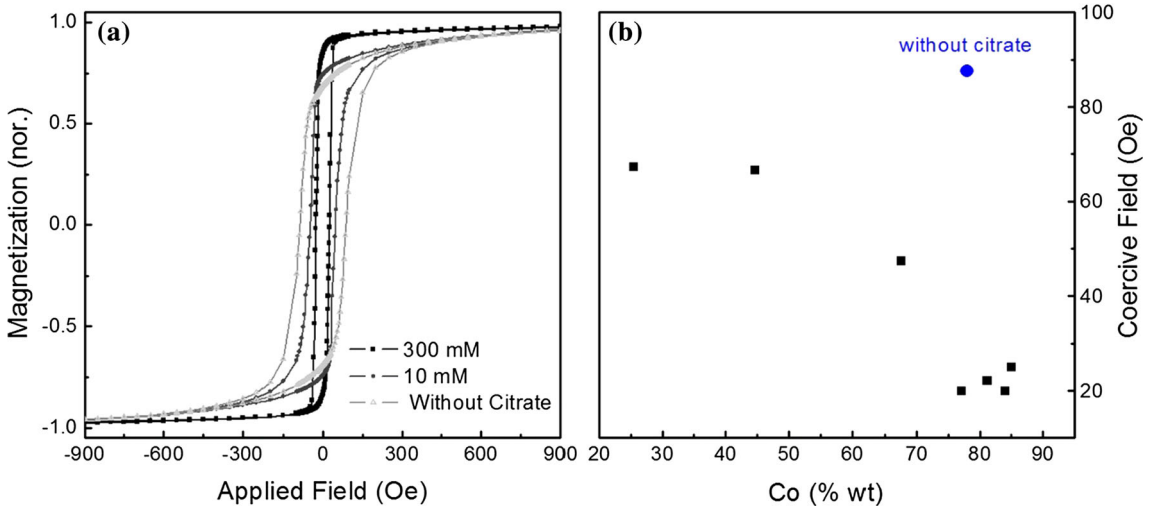

Fig. 3 **a** In-pane hysteresis loops for the samples electrodeposited at −1.0 V versus SCE in the absence (*triangle*) and with the addition of 10 mM (*circle*) and 300 mM (*square*) trisodium citrate. **b** Coercive field as function of Co contained in the samples electrodeposited at −1.0 V versus SCE

Table 1 Ratio of Co, Si wt% and Hc values obtained with changing the amount of citrate added to the electrolyte

Citrate (mM)	Co wt% (EDX)*		Si wt% (EDX)		Hc (Oe)	
	−0.95 V versus SCE	−1.00 V versus SCE	−0.95 V versus SCE	−1.00 V versus SCE	−0.95 V versus SCE	−1.00 V versus SCE
Free	43.26	77.49	42.86	42.51	124.6	87.5
2	55.67	25.20	66.15	52.53	39.0	67.2
4	58.41	43.61	62.14	47.05	21.7	66.5
10	69.75	67.59	42.31	46.24	18.5	47.4
30	71.31	77.23	40.35	41.14	19.5	21.9
120	74.93	83.20	37.75	43.28	18.5	22.0
200	70.37	83.96	38.25	44.36	19.6	19.9
300	66.67	85.02	39.39	42.47	37.3	24.9
450	53.62	76.62	54.15	58.03	65.9	–
600	15.76	51.32	74.07	83.39	–	–

* Relative percentages of Co and Cu were determined by making the detected amounts of the two metals equal to 100 % (Co wt% + Cu wt% = 100)

as indicated by the amount of Si detected, with 42 and 41 % Si, respectively. In spite of these similarities in Co content and thickness, these samples differ largely with regard to the measured coercive field owing to the improved film quality (see Fig. 1c–e) and change in crystalline structure induced by the citrate.

While the saturation magnetization depends primarily on the quantity and magnetic species in the sample, the coercive field, which in general gives information about the process of magnetization inversion, depends on structural factors. There are basically two possible mechanisms for the reversal to occur: (1) nucleation and growth of magnetic domain in the direction of the external field applied or (2) rotation of the domain in the direction of the external field. In thin films, the domain rotation is generally predominant. Structural defects act as pinning points for the rotation, and therefore higher external fields are necessary to overcome pinning. A good example of this phenomenon is the influence of surface roughness of Co thin films on the Hc [23]. On the other hand, the magnetocrystalline anisotropy depends on the material crystal structure and affects the Hc. Co may exhibit a cubic crystal structure with smaller Hc than those obtained for the hexagonal crystal structure [24], since the axis of easy magnetization is defined by the symmetry of each structure.

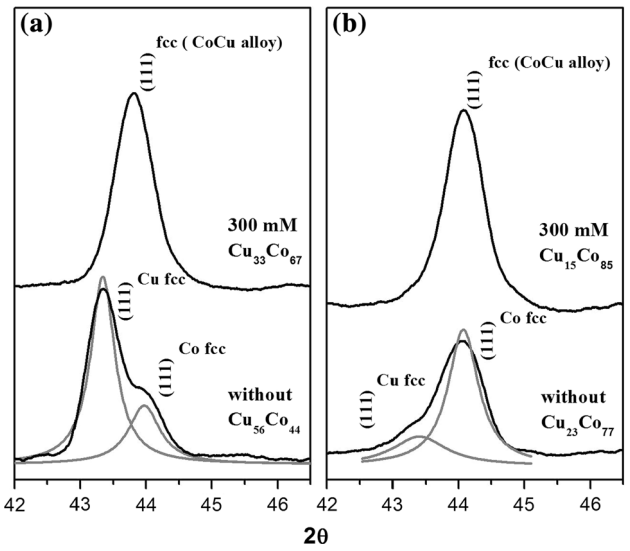

Fig. 4 XRD pattern of the of CuCo samples in the absence and with addition of 300 mM trisodium citrate, electrodeposited at **a** −0.95 V versus SCE and **b** −1.0 V versus SCE. The indexing of the peaks as reference standards was the ICDD database (00-008-0836) for Cu fcc and (00-015-0806) for Co fcc

The crystalline structure was analyzed by X-ray diffraction. Figure 4 shows the patterns for CuCo electrodeposited at −0.95 V versus SCE (Fig. 4a) and −1.0 V versus SCE (Fig. 4b) in the absence and presence of 300 mM trisodium citrate. The equilibrium phase diagram in the CoCu system indicates negligible solubility of two metals at room temperature [25, 26]. The electrodeposition is a nonequilibrium method and may be used to produce metastable solid solutions. Results show that the electrodeposited film without trisodium citrate has two distinct fcc crystalline structures, characteristic of Cu and Co separately, which is clear from the deconvolution of peak (111). The indexing of the peaks as reference standards was the ICDD database (00-008-0836) for Cu fcc and (00-015-0806) for Co fcc. The peak (111) is the most intense in the fcc phase, located at $2\theta = 43.298$ (for copper) and $2\theta = 44.217$ (for cobalt). In the results in Fig. 4 (without citrate), the majority phase is Cu fcc for the sample produced at −0.95 V versus SCE, whereas it is Co fcc for the sample produced at −1.0 V versus SCE, consistent with the composition of Cu and Co determined by EDX. In both cases phase segregation is evident. When the complexing agent trisodium citrate was used to promote simultaneous codeposition of copper and cobalt, only one symmetrical peak (111) was observed for the fcc phase for both deposition potentials used. The experimental data could not be fitted with two peaks; on the contrary, the position of the fitted peak is consistent with the solid solution of CuCo alloys.

Samples obtained without citrate consists of a heterogeneous system [25], with copper crystal grains dispersed in a cobalt matrix. These grains act as non magnetic impurities causing pinning in the rotation of the magnetic domains of cobalt. With the addition of citrate, a homogeneous system is formed by copper atoms replacing some of the cobalt atoms in the same crystal lattice. This may cause distortion in the lattice parameters, but does not hinder rotation of the domains.

4 Conclusions

The addition of trisodium citrate to the electrolyte turned out to be necessary to obtain films of excellent quality, high adhesion to the substrate and intense metallic sheen. An optimized citrate concentration of 300 mM was found to lead to the highest Co percentage in the films (for the potential of −1.0 V vs. SCE). In addition, changes in the electrolyte also reflected on the current efficiency. Therefore, increased saturation and remanence magnetizations and reduced coercive fields could be associated with stoichiometric variation in the samples. Regarding the crystalline structure, the films exhibited an overlap of the fcc phase for copper and cobalt when produced without the complexing agent. Through deconvolution of the (111) peak, two distinct structures, Co (111) and Cu (111), were identified. However, for the films prepared with trisodium citrate, only a fcc structure was identified which was related to a solid solution structure. The correlation between crystal structure and coercive field in the samples with the same percentage of Co shows that the coercive field of the solid solution was 20 Oe while for the sample with two fcc structures it was 87 Oe. It should be remarked that this high coercive field for the sample produced without citrate is due not only to phase segregation but also to a large film roughness. Taken together, the results presented here demonstrate that electroplating can yield good quality films, whose structural and magnetic properties can be controlled for tailored use in electronic devices such as sensors and data storage systems.

Acknowledgments The authors should thank the financial support from Conselho Nacional de Desenvolvimento Científico e Tecnológico (CNPq) (process 454704/2014-3 and Scholarship 158984/2014-5), for the financial support. The authors are grateful to Professor Dr[a] Maria Luisa Sartorelli and Professor Dr. Osvaldo Novaes de Oliveira for his support. They also acknowledge UFSC for the use of the LDRX-UFSC facilities for the X-ray diffraction experiments.

References

1. T. Cohen-Hyams, W.D. Kaplan, D. Aurbach, Y.S. Cohen, J. Yahalom, J. Electrochem. Soc. **150**, C28 (2003)

2. Y. Jyoko, S. Kashiwabara, Y. Hayashi, J. Electrochem. Soc. **144**, L5 (1997)
3. M.N. Baibich, J.M. Broto, A. Fert, F. Nguyen Van Dau, F. Petroff, P. Etienne, G. Creuzet, A. Friederich, J. Chazelas, Phys. Rev. Lett. **61**, 2472 (1988)
4. G. Binasch, P. Grünberg, F. Saurenbach, W. Zinn, Phys. Rev. B. **39**, 4828 (1989)
5. A.E. Berkowitz, J.R. Mitchell, M.J. Carey, A.P. Young, S. Zhang, F.E. Spada, F.T. Parker, A. Hutten, G. Thomas, Phys. Rev. Lett. **68**, 3745 (1992)
6. S. Kalsen, M. Alper, H. Kockar, M. Haciismailoglu, O. Karaagac, H. Kuru, J. Supercond. Nov. Magn. **26**, 813 (2013)
7. H. Jiazhi, C. Leng, J. Mater. Sci.: Mater. Electron. **26**, 3168 (2015)
8. E. Chassaing, K.V. Quang, R. Wiart, J. Appl. Electrochem. **16**, 591 (1986)
9. S. Rode, C. Henninot, C. Vallières, M. Matlosz, J. Electrochem. Soc. **151**, 405 (2004)
10. J. García, V.M. Prida, L.G. Vivas, B. Hernando, E.D. Barriga-Castro, R. Mendoza-Reséndez, C. Luna, J. Escrig, M. Vázquez, J. Mater. Chem. C **3**, 4688 (2015)
11. R. Hafizi, M.E. Ghazi, M. Izadifard, J. Supercond. Nov. Magn. **25**, 2737 (2012)
12. O. Karaagac, H. Kockar, M. Alper, IEEE Trans. Magn. **46**, 3973 (2010)
13. R. López Antón, M.L. Fdez-Gubieda, M. Insausti, A. Garcías-Arribas, J. Herreros, J. Non-Crystalline Solids **287**, 26 (2001)
14. E. Gómez, A. Labarta, A. Llorente, E. Vallés, J. Electroanal. Chem. **517**, 63 (2001)
15. E. Gómez, A. Llorente, E. Vallés, J. Electroanal. Chem. **495**, 19 (2000)
16. R.Y. Ying, P.K. Ng, Z. Mao, R.E. White, Electrochem. Soc. **135**, 2964 (1988)
17. E.J. Podlaha, Ch. Bonhôte, D. Landolt, Electrochim. Acta **39**, 2649 (1995)
18. S.S. Abd El Rehim, S.M. Abd El Wahaab, M.A.M. Ibrahim, M.M. Dankeria, J. Chem. Technol. Biot. **73**, 369 (1998)
19. N.C. Li, A. Lindenbaum, J.M. White, J. Inorg. Nucl. Chem. **12**, 122 (1959)
20. R. López Antón, M.L. Fdez-Gubieda, A. García-Arribas, J. Herreros, M. Insausti, Mat. Sci. Eng. A. **335**, 94 (2002)
21. M.R. Khelladi, L. Mentar, A. Azizi, L. Makhloufi, G. Schmerber, A. Dinia, J. Mater. Sci.: Mater. Electron. **23**, 2245 (2012)
22. U. Sarac, M.C. Baykul, J. Mater. Sci.: Mater. Electron. **25**, 39 (2014)
23. M.L. Munford, M.L. Sartorelli, L. Seligman, A.A. Pasa, J. Electrochem. Soc. **149**, 274 (2002)
24. M.S. Bhuiyan, B.J. Taylor, M. Paranthaman, J.R. Thompson, J.W. Sinclair, J. Mater. Sci. **43**, 1644 (2008)
25. E. Gómez, A. Llorente, X. Alcobe, E. Vallés, J. Solid State Electrochem. **8**, 82 (2004)
26. S. Ram, P.S. Frankwicz, Phys. Status Solidi A **188**, 1129 (2001)